Ion beam irradiation induced fabrication of vertical coupling waveguides

H. D. Liang (梁海东),[1,a)] V. S. Kumar,[1] J. F. Wu,[1] and M. B. H. Breese[1,2]
[1]*Centre for Ion Beam Applications (CIBA), Department of Physics, National University of Singapore, Singapore 117542*
[2]*Singapore Synchrotron Light Source (SSLS), 5 Research Link, National University of Singapore, Singapore 117603*

(Received 14 October 2012; accepted 26 March 2013; published online 5 April 2013)

Vertically coupled waveguides have been fabricated on a silicon-on-insulator platform using a combination of reactive ion etching to pattern the device layer and high-energy proton beam irradiation followed by electrochemical etching to pattern the substrate. Infra-red light can be coupled from the lower rib waveguide within the substrate into the upper waveguide within the device layer. By varying the proton energy along the lower waveguide, we have fabricated a tapered profile which is thin at the coupling region for higher efficiency and thicker towards the outer ends for easier coupling of light. A typical coupling efficiency of 26% has been achieved. © *2013 American Institute of Physics*. [http://dx.doi.org/10.1063/1.4801307]

Vertical coupling is a fundamental requirement for three-dimensional (3D) integrated photonic structures. Due to the limitation of conventional semiconductor machining techniques for producing multilayer structures, wafer bonding[1] or chemical vapor deposition (CVD)[2] and epitaxial growth techniques[3] are usually used. Another route is by using a modified SIMOX process,[4] involving patterned oxygen implantation. Using a wafer bonding approach, devices are fabricated on two separate chips, then the two aligned chips are attached. CVD is mainly used for deposition of organics to fabricate polymer devices. Epitaxial growth can help to fabricate heterostructure devices using semiconductors such as SiGe and GaAs. In this work, we demonstrate a process for fabricating vertical coupling photonic structures using a single silicon-on-insulator (SOI) wafer to give an all-silicon device.

High energy ions of a few hundred keV can penetrate many micrometers into semiconductor materials, such as Si and GaAs. In p-type silicon, a process has been developed to combine ion irradiation with subsequent electrochemical anodization to machine in 3D.[5,6] The flow of anodization current is deflected away from irradiated regions, leaving them unetched, surrounded by porous silicon. Most ion induced defects are located close to the end-of-range of the ions, so for low fluences only the end-of-range region remains unetched while regions closer to the surface become anodized. Thus by varying the ion energy, it is possible to directly fabricate 3D structures on Si and other semiconductors.[7] Here, we apply this process to make vertically coupled waveguides on a SOI wafer in conjunction with reactive ion etching (RIE).

SOI is widely used in photonics[8,9] as it provides an excellent platform for the fabrication of various photonic structures, with the advantage of high index contrast between Si and SiO_2 and full integration of electronic and optical devices on the same substrate. RIE is widely used in the fabrication of two-dimensional photonic structures[8,10] for surface patterning but cannot achieve patterning in 3D. We use RIE to pattern the SOI device layer and then pattern the substrate using our ion irradiation and etching process to fabricate multilayer structures, as shown in Fig. 1.

The SOI device layer is 230 nm thick, the buried oxide (BOX) layer is 145 nm thick, and the p-type substrate has a resistivity 14–22 Ω cm. First, we use UV lithography and RIE to fabricate the upper Si waveguides on the device layer, Fig. 1(c). After removing the first step photoresist, we spin coat another layer of photoresist and perform an aligned UV exposure to define the locations of the lower Si waveguides in the substrate. We then use proton beam irradiation, Fig. 1(d), to transfer the pattern of the lower waveguides on the photoresist into the substrate, forming a region containing ion induced defects both laterally and in depth. The defect distribution as a function of depth is determined by the proton beam energy.[5] For our purposes, the most relevant aspect is that defects are created along the full ion trajectory. After removing the photoresist, the sample is placed in a 24% HF solution for 1 min to chemically etch away the BOX layer to expose the substrate. The sample is then electrochemically anodized (current density of 60 mA/cm^2 for 1 min), Fig. 1(e). The porous Si (PSi) layer is then removed using a dilute KOH solution and a second electrochemical anodization (current density of 40 mA/cm^2 for 5 min) provides the PSi cladding of the bottom surface of the lower waveguide, Fig. 1(f). As a final step, the sample is annealed in low ambient pressure (∼1 mbar) at 500 °C for 10 h, to anneal out the ion induced defects while providing a small amount of oxidation-induced surface smoothening.[9,11]

Fig. 2 shows scanning electron micrographs (SEMs) of the final structure. Fig. 2(a) shows a plan view at low magnification where the curved, lower waveguide and straight, upper waveguide are seen. The upper waveguide is designed to be 3 mm long and free-standing. However, such a thin upper waveguide is not rigid enough to withstand such a long free-standing length, resulting in bending downwards towards the lower waveguide, giving a gap close to zero at the coupling region rather than equal to the BOX thickness. At either end of the coupling region, the upper waveguide is clearly bent, which contributes further losses. Such bending

[a)]Author to whom correspondence should be addressed. Electronic mail: g0900728@nus.edu.sg

 © 2013 American Institute of Physics

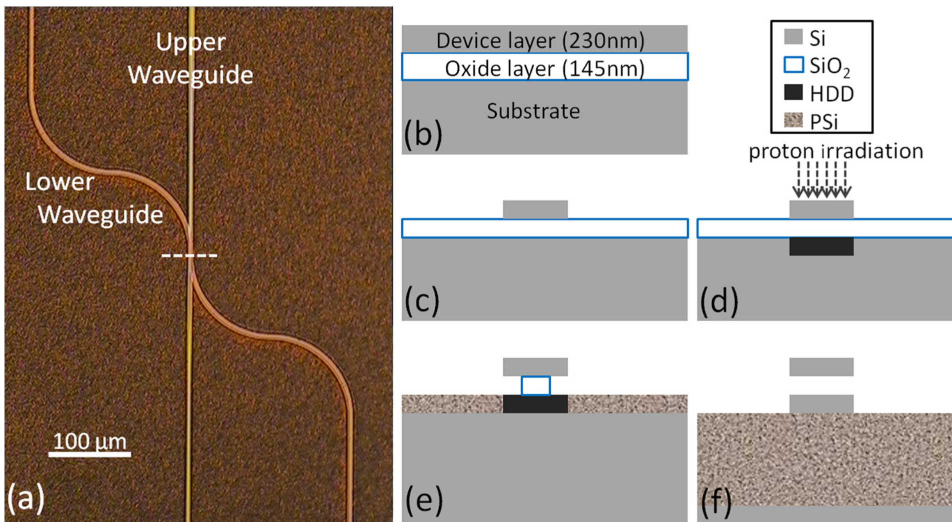

FIG. 1. (a) Optical micrograph showing an overview of the structure. (b)–(f) A schematic of the fabrication process viewed along a cross section at the dashed white line in (a). (b) SOI wafer dimensions, (c) RIE to fabricate the top Si waveguide (WG), (d) proton beam irradiation to create a high defect density (HDD) region for the lower waveguide in the substrate, (e) anodization resulting in oxide layer partial removal and PSi formation, (f) final anodization step to undercut the lower waveguide, followed by annealing to remove the lattice damage.

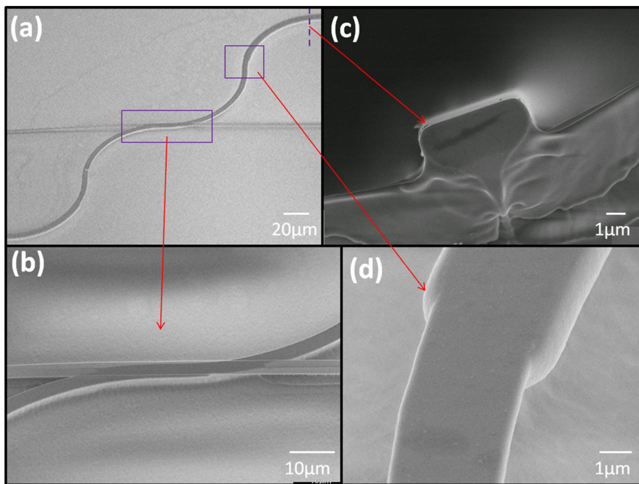

FIG. 2. SEM images of the structure, showing low magnification views of (a) the full structure and (b) the coupling region, (c) high magnification cross section of the thick lower waveguide ($\sim 5.4\,\mu m \times 2.5\,\mu m$), (d) plan view of the tapered portion of the lower waveguide.

could be mitigated by making a shorter free-standing length. The lower waveguide shown in Fig. 2 was irradiated by two different proton beam energies, 50 keV at the coupling region and 200 keV away from this region. Fig. 2(b) shows the coupling region, which is about 25 μm long in this case. Figs. 2(c) and 2(d), respectively, show a cross-section profile at one end of the lower waveguide and a plan view of the tapered portion between the two different proton beam energies used to fabricate it. The width of the lower waveguide is mainly determined by the photolithographic pattern and its thickness by the proton beam energy and fluence. A uniform proton beam current of 100 nA, distributed over an area of 1×1 cm^2, was used to irradiate the sample after photolithography[12] with a fluence of 2×10^{15} protons/cm^2. A 200 keV proton beam energy (range $\sim 1.9\,\mu$m in silicon, according to SRIM[13]) was used to produce a lower waveguide thickness of about 2.5 μm; such a thick waveguide allows easy coupling of light from a tapered optical fiber or focal lens but at the expense of a lower coupling efficiency into the upper waveguide. To improve the efficiency, a proton beam energy of 50 keV was used to irradiate the coupling region, the reduced energy producing a much thinner lower waveguide and consequently higher coupling efficiency, as described below.

Simulations were performed using RSoft[14] to better predict and understand the dependence of the coupling efficiency on the waveguide dimensions within the vertical structure. Fig. 3(a) shows a simplified schematic of the simulated structure. The incoming light wavelength is set as 1550 nm on changing it between 1530 nm and 1570 nm; the results are almost constant for a coupling length of 20 μm. As the device layer of the SOI wafer is fixed, the thickness of the upper waveguide is fixed at $T_U = 230$ nm. As discussed above, the two waveguides are almost in contact, so the gap between them is set as zero. Their width is designed as 4.5 μm. Experimentally, the proton beam energy which is used to define the lower waveguide can be varied in order to change its thickness T_L; in the simulations, we studied thicknesses from 0.1 μm to 2 μm. Fig. 3(a) shows the coupling efficiency of four different thicknesses ($T_L = 0.23\,\mu$m, 0.5 μm, 1 μm, 2 μm) along a coupling length of 11 μm. With $T_L = 0.23\,\mu$m, the simulated maximum coupling efficiency is over 90% within a coupling length of 1.2 μm. However, very accurate control over the dimensions is required to utilize such high coupling efficiency. For $T_L = 0.5\,\mu$m, the maximum coupling efficiency decreases to $\sim$35%, but the tolerance of the required dimensions increases. For $T_L = 1\,\mu$m and 2 μm, the coupling efficiency is below 10% and 2%, respectively. To summarize, when two waveguides are of a similar thickness, the maximum coupling efficiency is very high, and the maximum coupling efficiency rapidly decreases with increasing T_L. In simulations, a gap of 0.2 μm between the two layers of waveguides was found to produce strongly polarization-dependent results, whereas when the gap is close to zero, the polarization dependence is very weak.

According to simulation results, a thinner lower waveguide is necessary in order to increase the coupling efficiency. From SRIM, a lower proton energy of 50 keV can produce a lower waveguide thickness of about 200 nm at the coupling region. However, usually there is a "tail" remaining after electrochemical anodization, Fig. 2(c), which results in an almost triangular profile of the lower waveguide. In the simulations in Fig. 3(b), we incorporated a more realistic

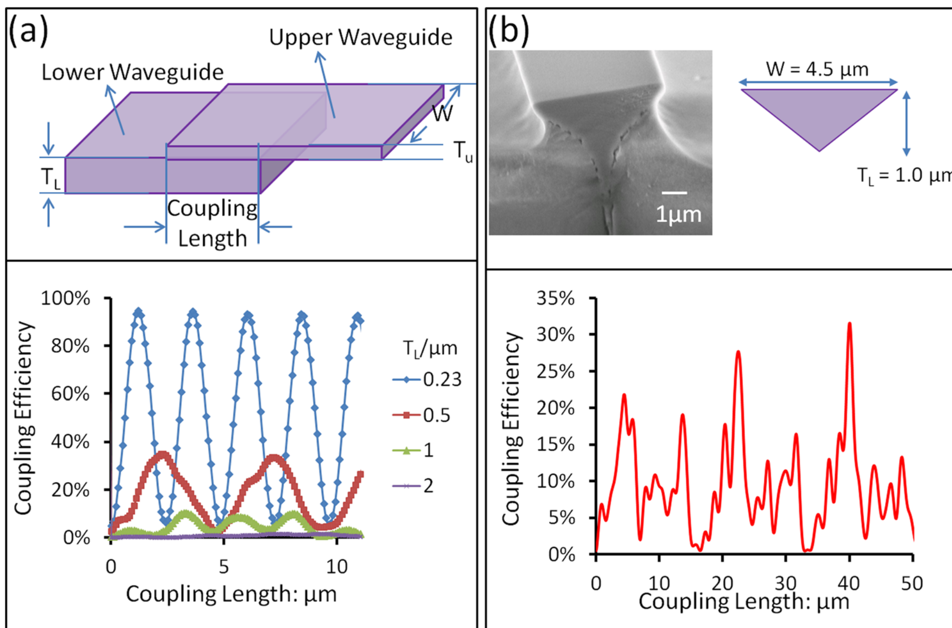

FIG. 3. Simulation results: (a) upper shows a schematic of the simulated structure, the waveguides width W and the upper waveguide thickness T_U are fixed. The two waveguides are attached, the lower waveguide thickness T_L is varied. (a) lower: plots the coupling efficiency for different T_L along a coupling length of 11 μm. (b) Upper shows the actual triangular profile of the lower waveguide and simplified triangular profile used in the simulation. (b) lower: plots the coupling efficiency of this profile along a coupling length of 50 μm.

triangular profile of the lower waveguide, having a width of 4.5 μm and a maximum thickness of 1 μm. With such a triangular profile, the coupling efficiency reaches around 27% at a coupling length of 22 μm, which is higher than what would typically be achieved for a uniform thickness of $T_L = 1\ \mu$m in Fig. 3(a). If necessary, this tail portion may be removed by reducing the width of the lower waveguide from its present value to $\sim$1 μm, based on our previous experience.[6]

Optical characterization was carried out in both TE and TM polarizations with a broad band source from 1530 nm to 1570 nm. A broad band laser was coupled into the waveguide using a 60× objective lens. A polarizing beam splitter and a half-wave plate before the objective lens enabled selection of TE or TM polarization. A InGaAs IR camera was used to monitor the scattered light from the top of the sample. Use of a tunable diode laser with a single wavelength at 1530 nm, 1540 nm, 1550 nm, 1560 nm, 1570 nm coupled into the bottom waveguide gave similar coupling efficiency as the broad band light source.

When the lower waveguide has a sub-micron thickness at the coupling region, Fig. 4 shows light coupling between the two layers of waveguides, viewing the scattered light from the top of the device and scattered light intensity measurements along the waveguides. Along the thin portion of the lower waveguide (A to B and C to D), there is more scattered light, in keeping with a thinner, curved geometry. However, measurement of scattered light from this portion is also influenced by its proximity to the coupling region, where a high background intensity of scattered light surrounding this region is observed. Because of this, the closest data points on either side of the coupling region are deemed to be not valid for the purpose of measuring the coupling efficiency, so are not joined to the main curve. The measured coupling efficiency of 26% ± 10% is defined as the (Input-Output1)/Input, with the values of I (Input) and O_1 (Output1) chosen as the average of the two valid data points in Fig. 4 which are close to the coupling region, within the zones A to B and C to D. For other similarly fabricated samples, we measured coupling efficiencies ranging from 16% to 35% with single wavelengths or broad band light, compared to only $\sim$3% measured in a sample where the lower waveguide was much thicker ($\sim$2.5 μm) at the coupling region. We believe that the measured variations of the coupling efficiency largely arise from limitations of the normal UV lithography and UV alignment. The coupling efficiency is similar to that achieved using a typical grating coupler.[15] The loss from the upper waveguide could be reduced with a shorter free-standing length and optimization of the UV lithography and RIE steps.

The propagation loss is measured by measuring the scattered light along a 3 mm length for the lower waveguide and a 1 mm length for the upper waveguide. Light was injected into each one in turn, with the coupling region playing no part in the measurements. From the measurements, losses of $\sim$3 dB/cm for the thick lower waveguide and $\sim$60 dB/cm for the upper waveguide were recorded. The loss of $\sim$60 dB/cm through the upper waveguide is significant, presumably

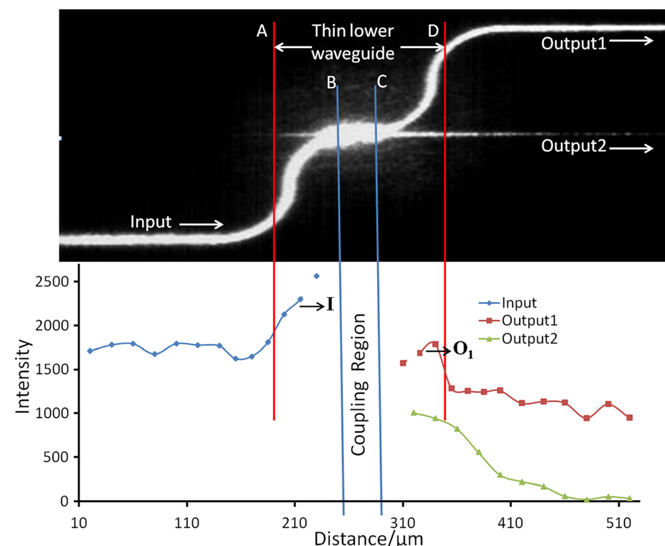

FIG. 4. IR image and scan of the scattering light intensity along the waveguides.

arising from its high roughness. Along the lower waveguide, there are two different parts: the thin coupling region and the thick portion away from the coupling region. The measured loss is that of the thick portion as the thin portion is short, curved and some portion of it interacts with the upper waveguide at the coupling region, making a meaningful loss measurement very difficult. However, from the straight end of Input to the straight beginning of Output1, a total loss of ∼32% was measured, so apart from a 26% coupling, it suggests a total loss of 6%, including the tapering loss, bending loss, and propagation loss through the whole thin part.

In conclusion, a process for fabricating vertically coupled structures using a combination of RIE and proton beam irradiation followed by an electrochemical etching of an SOI wafer is demonstrated. Reasonably efficient light coupling of ∼16% to 35% between the two layers of waveguides was obtained. Further work is aimed at optimizing the fabrication process to improve the repeatability of the coupling efficiency using deep UV alignment. Such vertically coupled waveguides could work as vertical-coupling directional splitters or as simple, high-efficiency vertical-couplers, and the same fabrication process can be further applied to fabricate other vertical coupling structures such as waveguide-to-microresonators.

[1]D. V. Tishinin, P. D. Dapkus, A. E. Bond, I. Kim, C. K. Lin, and J. O'Brien, IEEE Photon. Technol. Lett. **11**(8), 1003 (1999); M.-C. M. Lee and M. C. Wu, Opt. Express **14**(11), 4703 (2006).
[2]K. Worhoff, P. V. Lambeck, and A. Driessen, J. Lightwave Technol. **17**(8), 1401 (1999).
[3]S. J. Choi, K. Djordjev, C. Sang Jun, P. D. Dapkus, W. Lin, G. Griffel, R. Menna, and J. Connolly, IEEE Photon. Technol. Lett. **16**(3), 828 (2004).
[4]P. Koonath, T. Indukuri, and B. Jalali, Appl. Phys. Lett. **86**(9), 091102 (2005).
[5]M. B. H. Breese, F. J. T. Champeaux, E. J. Teo, A. A. Bettiol, and D. J. Blackwood, Phys. Rev. B **73**(3), 035428 (2006).
[6]E. J. Teo, A. A. Bettiol, P. Yang, M. B. H. Breese, B. Q. Xiong, G. Z. Mashanovich, W. R. Headley, and G. T. Reed, Opt. Lett. **34**(5), 659 (2009).
[7]S. Azimi, M. B. H. Breese, Z. Y. Dang, Y. Yan, Y. S. Ow, and A. A. Bettiol, J. Micromech. Microeng. **22**(1), 015015 (2012); F. Menzel, D. Spemann, and T. Butz, Nucl. Instrum. Methods Phys. Res. B **269**(20), 2457 (2011).
[8]P. Dumon, W. Bogaerts, V. Wiaux, J. Wouters, S. Beckx, J. Van Campenhout, D. Taillaert, B. Luyssaert, P. Bienstman, D. Van Thourhout, and R. Baets, IEEE Photon. Technol. Lett. **16**(5), 1328 (2004).
[9]K. K. Lee, D. R. Lim, L. C. Kimerling, J. Shin, and F. Cerrina, Opt. Lett. **26**(23), 1888 (2001).
[10]T. Baba, Nat. Photonics **2**(8), 465 (2008).
[11]E. J. Teo, B. Q. Xiong, Y. S. Ow, M. B. H. Breese, and A. A. Bettiol, Opt. Lett. **34**(20), 3142 (2009).
[12]D. Mangaiyarkarasi, Y. S. Ow, M. B. H. Breese, V. L. Fuh, and E. T. Xioasong, Opt. Express **16**(17), 12757 (2008).
[13]J. F. Ziegler, J. P. Biersack, and U. Littmark, *The Stopping and Range of Ions in Solids* (Pergamon, 1985); J. F. Ziegler, M. D. Ziegler, and J. P. Biersack, Nucl. Instrum. Methods Phys. Res. B **268**(11–12), 1818 (2010).
[14]S. P. Chan, C. E. Png, S. T. Lim, G. T. Reed, and V. M. N. Passaro, J. Lightwave Technol. **23**(6), 2103 (2005).
[15]S. Scheerlinck, D. Taillaert, D. Van Thourhout, and R. Baets, Appl. Phys. Lett. **92**(3), 031104 (2008); D. Taillaert, F. Van Laere, M. Ayre, W. Bogaerts, D. Van Thourhout, P. Bienstman, and R. Baets, Jpn. J. Appl. Phys., Part 1 **45**(8A), 6071 (2006).